

# Identification of New Modulators and Inhibitors of Palmitoyl-Protein Thioesterase 1 for CLN1 Batten Disease and Cancer

Ana C. Puhl, Renuka Raman, Tammy M. Havener, Eni Minerali, Anthony J. Hickey, and Sean Ekins\*



Cite This: *ACS Omega* 2024, 9, 11870–11882



Read Online

ACCESS |



Metrics & More

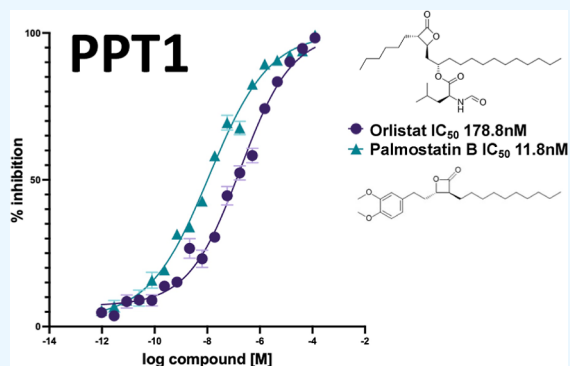


Article Recommendations



Supporting Information

**ABSTRACT:** Palmitoyl-protein thioesterase 1 (PPT1) is an understudied enzyme that is gaining attention due to its role in the depalmitoylation of several proteins involved in neurodegenerative diseases and cancer. PPT1 is overexpressed in several cancers, specifically cholangiocarcinoma and esophageal cancers. Inhibitors of PPT1 lead to cell death and have been shown to enhance the killing of tumor cells alongside known chemotherapeutics. PPT1 is hence a viable target for anticancer drug development. Furthermore, mutations in PPT1 cause a lysosomal storage disorder called infantile neuronal ceroid lipofuscinosis (CLN1 disease). Molecules that can inhibit, stabilize, or modulate the activity of this target are needed to address these diseases. We used PPT1 enzymatic assays to identify molecules that were subsequently tested by using differential scanning fluorimetry and microscale thermophoresis. Selected compounds were also tested in neuroblastoma cell lines. The resulting PPT1 screening data was used for building machine learning models to help select additional compounds for testing. We discovered two of the most potent PPT1 inhibitors reported to date, orlistat (IC<sub>50</sub> 178.8 nM) and palmotatin B (IC<sub>50</sub> 11.8 nM). When tested in HepG2 cells, it was found that these molecules had decreased activity, indicating that they were likely not penetrating the cells. The combination of in vitro enzymatic and biophysical assays enabled the identification of several molecules that can bind or inhibit PPT1 and may aid in the discovery of modulators or chaperones. The molecules identified could be used as a starting point for further optimization as treatments for other potential therapeutic applications outside CLN1 disease, such as cancer and neurological diseases.



## INTRODUCTION

Lysosomal storage diseases (LSDs) are a collection of more than 70 clinical syndromes caused by mutations in approximately 50 genes encoding proteins necessary for lysosomal function, and in most cases, they represent enzymes involved in the cellular degradation and trafficking of lipids and other macromolecules.<sup>1</sup> This deficiency of a lysosomal function then leads to the accumulation of a wide range of complex substrates<sup>2</sup> and the secondary impairment of lysosome-related pathways.<sup>1</sup> Approximately 70% of LSD is present as a progressive neurodegenerative disease, highlighting how vulnerable the central nervous system (CNS) is to lysosomal dysfunction.<sup>3</sup> The infantile neuronal ceroid lipofuscinosis (CLN1 disease) is an LSD caused by mutations in CLN1, which encodes for palmitoyl-protein thioesterase 1 (PPT1).<sup>4</sup> CLN1 disease is characterized by progressive neurodegeneration, blindness, and seizures and is ultimately fatal in childhood. Age of onset can vary greatly depending on the type of CLN1 mutation; where patients homozygous for null mutations display more severe disease symptoms in infancy. Animal models missing or deficient in PPT1 display neuronal loss, astrocytosis, microglial activation, motor deficits, and early death.<sup>5,6</sup> There is also accumulating evidence that the lack of PPT1 impacts glial activation, presynaptic vesicle dysfunction,

and postsynaptic deficits in NMDA receptor maturation.<sup>7,8</sup> Missense mutations that result in complete but misfolded proteins, however, open the possibility of rescuing enzymatic activity using pharmacological chaperones. These are ideally small molecules that reversibly bind to a protein and stabilize its structure, forming a correctly folded protein long enough to be trafficked out of the ER without being flagged for degradation.<sup>9,10</sup> Pharmacological chaperone therapy (PCT) uses these small molecule active site-specific inhibitors to stabilize the conformation of the mutant protein in order to increase the level of the residual activity to a point sufficient to reverse the clinical phenotype.<sup>10</sup> This observation is a foundation for drug development for all enzymes including those involved in LSD.<sup>11–13</sup> Restoration of 3–5% of the enzyme activity has been shown to slow down the clinical progress of the disease for several LSDs.<sup>14,15</sup> Following

**Received:** December 1, 2023

**Revised:** February 2, 2024

**Accepted:** February 13, 2024

**Published:** February 28, 2024



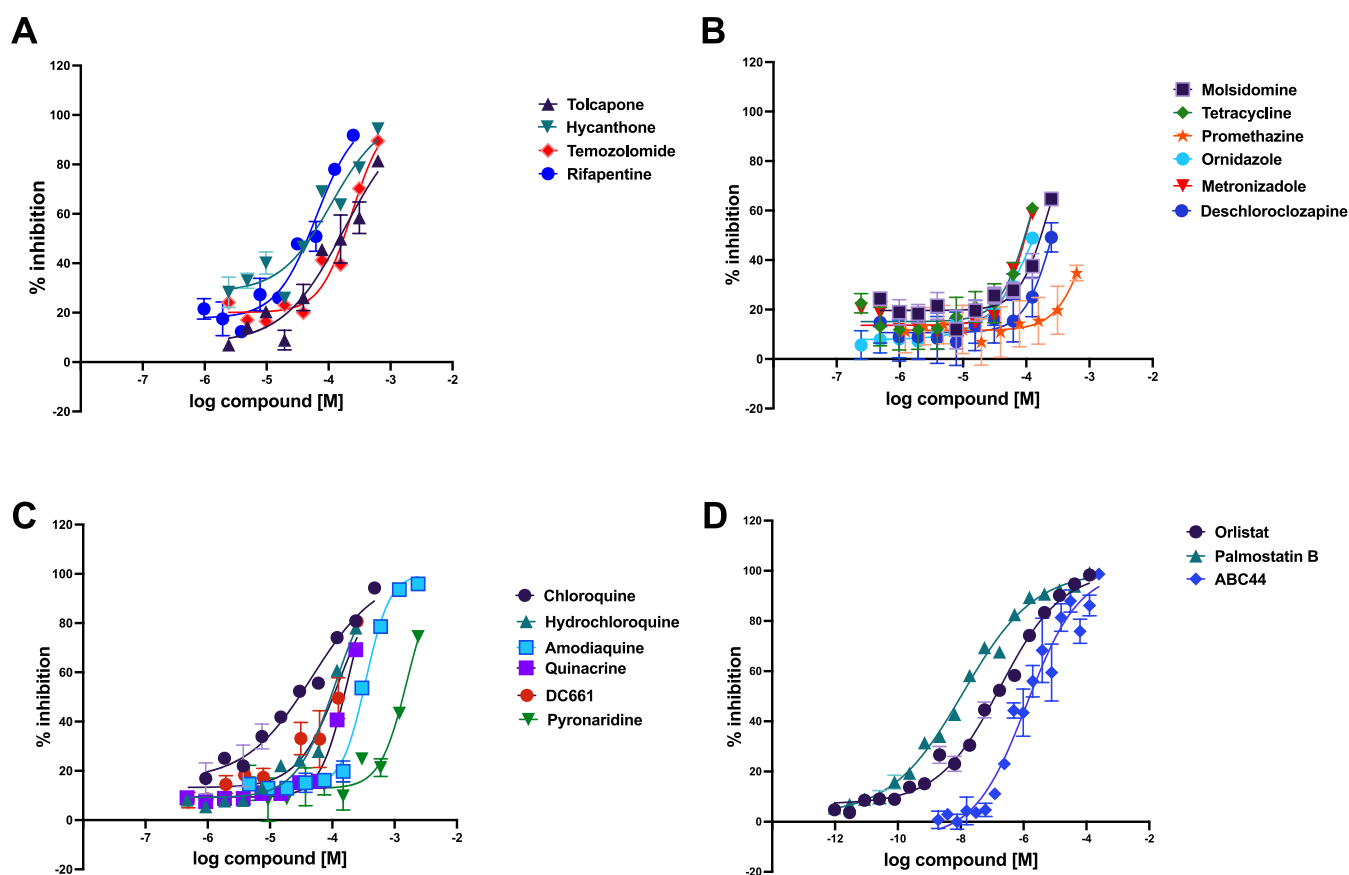


**Figure 1.** PPT1 enzyme activity inhibition. (A) Tolcapone  $IC_{50}$  179.1  $\mu M$  (97–275  $\mu M$ ), hycanthone  $IC_{50}$  110.8  $\mu M$  (57–179  $\mu M$ ), temozolomide  $IC_{50}$  236  $\mu M$  (183–300  $\mu M$ ), and rifapentine  $IC_{50}$  63.3  $\mu M$  (46–84  $\mu M$ ). (B) Molsidomine, tetracycline, promethazine, ornidazole, metronidazole, and deschloroclozapine ( $IC_{50}$  was not calculated because dose–response curves did not reach a plateau). (C) Antimalarials and derivatives: chloroquine  $IC_{50}$  47.2  $\mu M$  (27–70  $\mu M$ ), hydroxychloroquine  $IC_{50}$  109.1  $\mu M$  (91–130  $\mu M$ ), amodiaquine  $IC_{50}$  344  $\mu M$  (318–373  $\mu M$ ), quinacrine  $IC_{50}$  estimated 169.4  $\mu M$  (150–192  $\mu M$ , curve did not reach the plateau), DC661  $IC_{50}$  129.6  $\mu M$  (103–161  $\mu M$ , curve did not reach the plateau), and pyronaridine  $IC_{50}$  estimated >125  $\mu M$  (curve did not reach the plateau). (D) Orlistat  $IC_{50}$  178.8 nM (136–232 nM), palmostatin B  $IC_{50}$  11.8 nM (8.7–15.6 nM), and ABC44  $IC_{50}$  1.26  $\mu M$  (0.66–2.11  $\mu M$ ).

preclinical in vitro and in vivo studies, chaperone therapies can be translated to clinical trials (Table S1), either as monotherapy or in combination with an enzyme replacement therapy for some of the most prevalent LSDs.<sup>3,14,16</sup>

Peptide mimics of PPT1 substrates have been used to stabilize a mutant PPT1 that carried a T75P missense mutation that displays low levels of enzyme activity in lymphoblastoid cell lines, increasing the enzymatic activity twofold.<sup>17</sup> PPT1 is a soluble lysosomal depalmitoylation enzyme, which removes long-chain fatty acids from modified cysteine residues in proteins.<sup>18</sup> The homeostasis of protein palmitoylation and depalmitoylation is therefore essential in the CNS for normal physiological function.<sup>19,20</sup> PPT1 might have additional physiological functions outside of lysosomes as proteomics analyses have repeatedly demonstrated the presence of PPT1 in synaptosomes.<sup>21–23</sup> Depalmitoylation by PPT1 is involved in several cellular processes, including those related to the autophagy–lysosome pathway, but it is especially important in neurons, where PPT1 contributes to axonal outgrowth, neurite extension, and dendritic spine morphogenic pathways.<sup>20,24–26</sup> A few protein substrates of PPT1 have additionally been identified, such as glial fibrillary acidic protein, and hyperpalmitoylation of this exacerbates astrogliosis and neurodegenerative pathology in PPT1-deficient mice.<sup>27</sup> In addition, PPT1 depalmitoylates the F1 complex of the mitochondrial

ATP synthase and is required for proper localization.<sup>20,28</sup> PPT1 depalmitoylates the V-ATPase component, V0a1,<sup>29</sup> and inhibitors of PPT1 can suppress autophagy.<sup>30</sup> The Src family kinase Fyn is a substrate of PPT1,<sup>20,31</sup> while Fyn is one of the many kinases known to phosphorylate tau,<sup>32</sup> suggesting that PPT1 inhibition and Fyn activity/localization should be investigated further for therapeutic applications in diseases such as Alzheimer's disease. It has been suggested that depalmitoylation by PPT1 is involved in the developmental switch of regulatory subunits of the *N*-methyl-D-aspartate receptor (NMDAR) from GluN2B to GluN2A and that this switch is disrupted in CLN1 disease.<sup>20</sup> Importantly, dynamic palmitoylation of GABA-synthesizing enzyme glutamic acid decarboxylase 65 (GAD65) regulates its trafficking and delivery to synapses.<sup>33</sup> SNAP25 and VAMP2 are also suggested to be substrates of PPT1 at the presynapse.<sup>34</sup> Despite the primary role of PPT1 in CLN1 disease, and its activity in depalmitoylation of protein substrates involved in several cellular processes, only a few inhibitors and molecules that bind PPT1 have been described to date,<sup>35</sup> which includes a peptide combined with palmitate, an *N*-hydroxyhydantoin carbamate inhibitor ABC44, as well as chloroquine and its derivatives.<sup>17,36,37</sup> Currently there are no small molecule or biologic treatments that have regulatory approval and are clinically available for CLN1 Batten disease treatment.

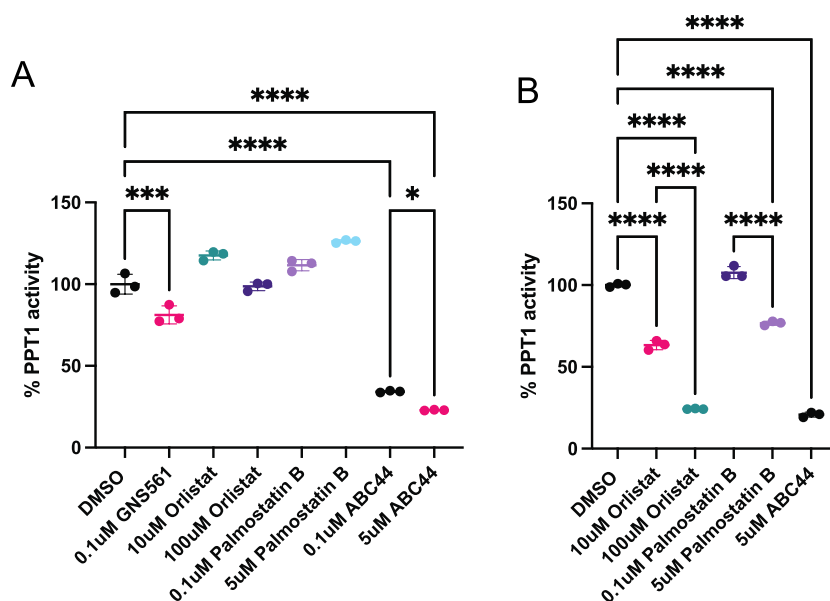


**Figure 2.** PPT1 inhibition in HepG2 cells and cell extracts. Inhibition of PPT1 enzyme activity in (A) HepG2 cells post-treatment with compounds for 5 h and (B) HepG2 cell extracts post-treatment with compounds for 1 h. Note: \* $p < 0.05$ , \*\* $p < 0.01$ , \*\*\* $p < 0.001$ , \*\*\*\* $p < 0.0001$ .

PPT1 has been characterized in SH-SY5Y human neuroblastoma cells and proteomic analysis performed,<sup>38</sup> which indicated the involvement of PPT1 in neuronal migration and the dopamine receptor-mediated signaling pathway. These early studies showed that PPT1 protects against apoptosis mediated by the Ras-Akt-Caspase pathway in neuroblastoma cells inferring that protein palmitoylation could regulate apoptosis.<sup>39</sup> PPT1 is hence an important underutilized target for cancer, and inhibitors lead to cell death and have been shown to kill tumor cells, enhancing the killing of neurotumor cells alongside known chemotherapeutics.<sup>40,41</sup> Tumor expression of PPT1 is associated with shorter overall survival in a variety of cancers including cholangiocarcinoma, esophageal cancer, head and neck cancer, renal cell carcinoma, and hepatocellular cancer.<sup>37</sup>

We have now employed several biochemical, biophysical, and computational techniques in an effort to identify new molecules that bind, stabilize, or inhibit PPT1. We have identified several molecules that have the potential to be further studied as small molecule modulators for CLN1 disease, cancer, and other neurological diseases.

## RESULTS

**High-Throughput Screening and IC<sub>50</sub> Determination.** Initially, we performed a screen to identify small molecule inhibitors of PPT1 using an enzymatic assay with a fluorogenic substrate 4-methylumbelliferyl-6-thio-palmitate- $\beta$ -D-glucopyranoside.<sup>42</sup> This substrate is cleaved by PPT1 to release the fluorescent moiety 4-methylumbelliferyl (4-MU). Initially, we calculated  $K_m$  for the substrate at 37 °C (Figure S1). We ultimately screened 2180 compounds at a substrate concentration of 20  $\mu$ M from the Spectrum Collection library using an enzymatic assay, where 40 compounds yielded >60% inhibition, as shown in Table S1. We followed these hits up with dose–response curves (Figure 1A) for hycanthone with an IC<sub>50</sub> of 110.8  $\mu$ M (range 57–179  $\mu$ M), temozolomide with an IC<sub>50</sub> of 236  $\mu$ M (183–300  $\mu$ M), and rifapentine with an IC<sub>50</sub> of 63.3  $\mu$ M (46–84  $\mu$ M). The dose–response curves for the molsidomine, tetracycline, promethazine, ornidazole,

metronidazole, and deschloroclozapine did not reach the plateau and IC<sub>50</sub> values were not calculated, but instead the values were estimated to be >100  $\mu$ M (Figure 1B). We additionally tested tolcapone, IC<sub>50</sub> 179.1  $\mu$ M (97–275  $\mu$ M), instead of entacapone which was identified in the initial screening, because tolcapone can penetrate the blood–brain barrier (BBB) and has a longer half-life.<sup>43</sup>

Besides the compounds identified in the initial enzymatic screening, we also investigated the in vitro activity of several known antimalarial compounds against PPT1 as it has been previously reported that PPT1 is the target for chloroquine and derivatives in cancer.<sup>37</sup> Although these compounds have been reported to have activity in cancer cell lines,<sup>37</sup> to our knowledge, the IC<sub>50</sub> with the purified PPT1 enzyme has not been reported. We demonstrated that chloroquine inhibits PPT1 with an IC<sub>50</sub> of 47.2  $\mu$ M (27–70  $\mu$ M), hydroxychloroquine IC<sub>50</sub> 109.1  $\mu$ M (91–130  $\mu$ M), amodiaquine IC<sub>50</sub> 344  $\mu$ M (318–373  $\mu$ M), quinacrine IC<sub>50</sub> estimated 169.4  $\mu$ M (150–192  $\mu$ M, curve did not reach the plateau), DC661 estimated IC<sub>50</sub> 129.6  $\mu$ M (103–161  $\mu$ M, curve did not reach plateau), and pyronaridine IC<sub>50</sub> estimated >125  $\mu$ M (curve did not reach plateau) (Figure 1C). We also tested other antimalarials such as proguanil, quinine, and mefloquine; however, none of these showed activity above 50% inhibition at 125  $\mu$ M (Table S3). Finally, we screened additional compounds from our in-house library and explored whether natural products could inhibit PPT1 activity (Table S2). Of these, only rutin trihydrate and vanillin inhibited PPT1 activity, with an IC<sub>50</sub> estimated 156  $\mu$ M (88–204  $\mu$ M) and IC<sub>50</sub> 647  $\mu$ M (434–819  $\mu$ M), respectively (Figure S2).

From this screen, orlistat was the most potent inhibitor (90.7%), which had an IC<sub>50</sub> of 178.8 nM (136–232 nM) (Figure 1D). We also evaluated a previously reported PPT1 inhibitor ABC44,<sup>36</sup> which had an IC<sub>50</sub> of 1.26  $\mu$ M in our assay (0.66–2.11  $\mu$ M). As orlistat is an irreversible inhibitor of pancreatic and gastric lipase, as well as an inhibitor of fatty acid synthase (FASN)<sup>44</sup> (IC<sub>50</sub> 1.35  $\mu$ M),<sup>45</sup> we evaluated additional inhibitors of FASN such as FT113, TVB-3166, and GSK2194069; however, they did not inhibit PPT1 (Table

Table 1. Summary of Compounds Tested in Enzymatic Assays, NanoDSF, MST, and in the Neuroblastoma SH-SY5Y Cell Line<sup>b</sup>

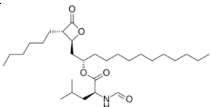
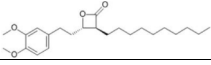
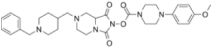
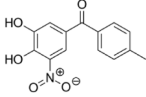
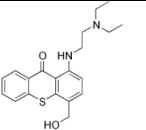
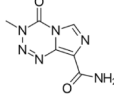
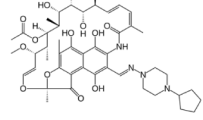
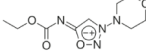
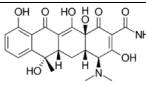
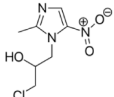
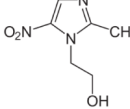
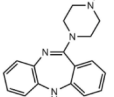
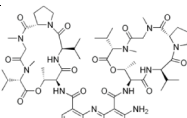
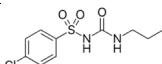
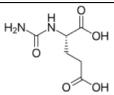
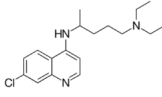
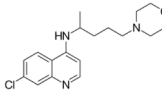
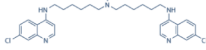
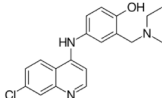
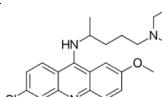
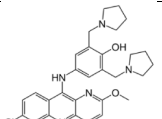
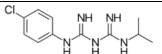
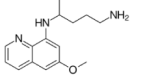
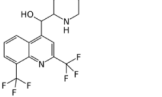
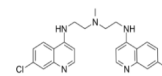
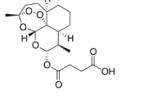
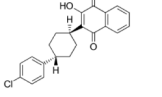
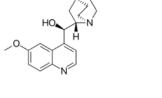
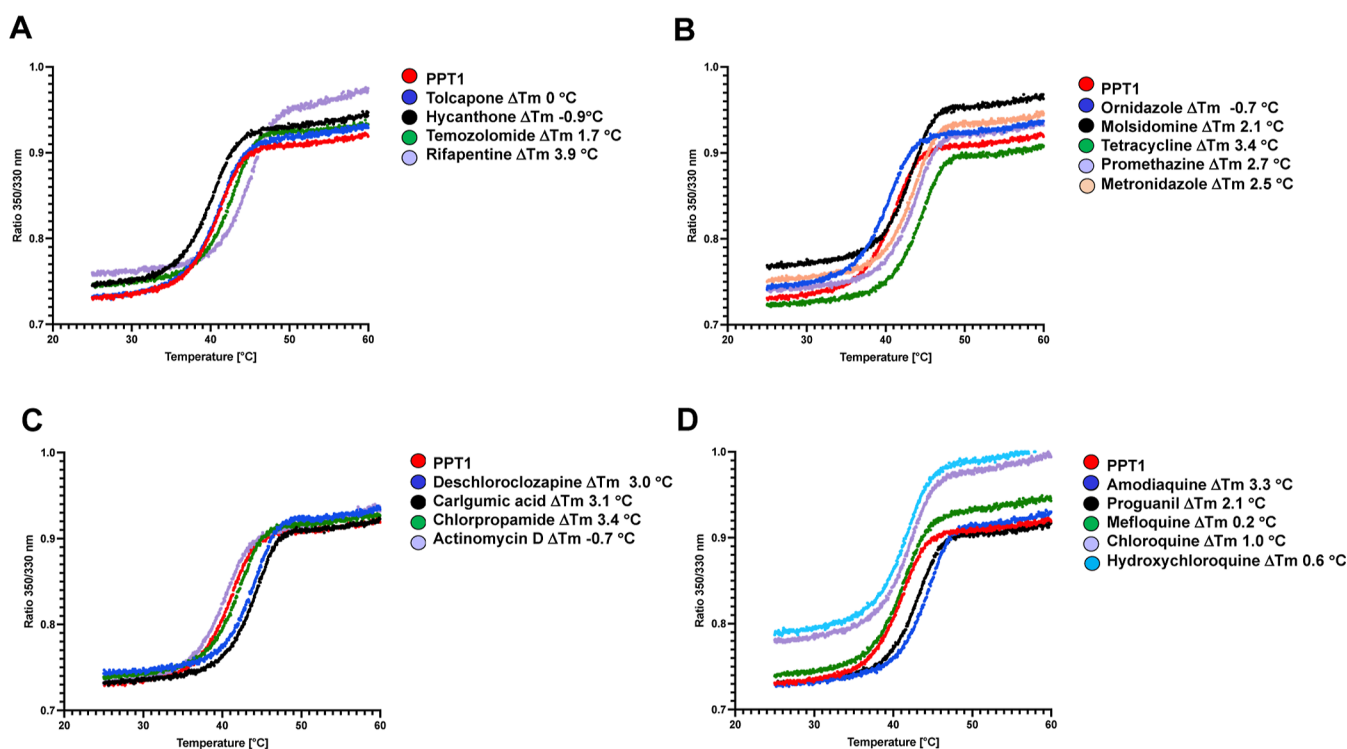
Structure	Compound	IC <sub>50</sub> (95 % CI)	ΔTm	MST (nM)	SH-SY5Y (IC <sub>50</sub> μM)
	Orlistat	178.8 nM (136 – 232 nM)			
	Palmostatin B	11.8 nM (8.7 – 15.6 nM)			
	ABC44	1.26 μM (0.66 – 2.11 μM)			
	Tolcapone	179.1 μM (97 – 275 μM)	0		NA
	Hycanthone	110.8 μM (57 – 179 μM)	-0.9		NA
	Temozolomide	236 μM (183 – 300 μM)	1.7		NA
	Rifapentine	63.3 μM (46 – 84 μM)	3.9		NA
	Molsidomine	*	2.1		NA
	Tetracycline	*	3.4		NA
	Promethazine	*	2.7		NA
	Ornidazole	*	-0.7		NA
	Metronidazole	*	2.5		NA
	Deschloroclozapine	*	3.0		NA
	Actinomycin D	*	-0.7	235 ± 107	NA
	Chlorpropamide	*	3.4	201 ± 50	NA

Table 1. continued

Structure	Compound	IC <sub>50</sub> (95 % CI)	ΔTm	MST (nM)	SH-SY5Y (IC <sub>50</sub> μM)
	Carglumic acid	*	3.1	1270 ± 740	NA
	Chloroquine	47.2 μM (27 – 70 μM)	1.0		44
	Hydroxychloroquine	109.1 μM (91 - 130 μM)	0.6		>50
	DC661	129.6 μM (103 – 161 μM)			
	Amodiaquine	344 μM (318 - 373 μM)	3.3	76 ± 36	17
	Quinacrine	estimated 169.4 μM (150 – 192 μM)			
	Pyronaridine	estimated > 125 μM			NA
	Proguanil	NA	2.1	808 ± 261	>50
	Primaquine				>50
	Mefloquine	NA, potential fluorescence problems	0.2	226 ± 90	8
	Lys05				9.5
	Artesunate				4.6
	Atovaquone				>50
	Quinine	NA, potential fluorescence problems		256 ± 107	NA

<sup>a</sup>IC<sub>50</sub> values were not calculated because dose–response curves did not reach a plateau. <sup>b</sup>NA = not active.



**Figure 3.** Thermal shift experiments. PPT1 (5  $\mu\text{M}$ ) in PBS + 1 mM BME was tested against compounds (50  $\mu\text{M}$ ). (A) Tolcapone, hycanthone, temozolomide, and rifapentine. (B) Ornidazole, molsidomine, tetracycline, promethazine, and metronidazole. (C) Deschloroclozapine, carlgumic acid, chlorpropamide, and actinomycin D. (D) Amodiaquine, proguanil, mefloquine, chloroquine, and hydroxychloroquine.

S3). We also tested a structurally related compound to orlistat, namely, palmostatin B, which is an acyl-protein thioesterase APT1 and APT2 inhibitor,<sup>46</sup> and this compound demonstrated inhibition of PPT1 with an  $\text{IC}_{50}$  of 11.8 nM (8.7–15.6 nM) (Figure 1D).

**Inhibition of PPT1 Activity of Orlistat and Palmostatin B in Cells.** To test PPT1 inhibition in cells, we performed a cell-based assay using HepG2 cells. Cells were treated with either DMSO, orlistat, palmostatin B, or ABC44 for 5 h, followed by the PPT1 enzyme activity assay from cell lysates. GNS561, a clinical-stage PPT1 inhibitor, was used as a positive control for the assay. GNS561 has previously been shown to inhibit PPT1 in a time-dependent manner (25% inhibition at 1  $\mu\text{M}$  after 3 h and 50% inhibition at 1  $\mu\text{M}$  after 72 h) and is the first PPT1 inhibitor to reach clinical trials.<sup>47</sup> The percent of PPT1 activity was determined relative to that of the DMSO control (Figure 2A, SA). Orlistat and palmostatin B exhibited poor PPT1 inhibition, whereas ABC44, a known PPT1 inhibitor, exhibited potent PPT1 inhibition. We hypothesized that the poor PPT1 inhibition exhibited by orlistat and palmostatin B was likely due to poor cell penetration since both of them are highly hydrophobic in nature. In order to test our hypothesis, we also treated HepG2 cell extracts, instead of intact cells with these compounds. Orlistat and palmostatin B inhibited PPT1 in cell extracts when treated for 1 h (Figure 2B, SB). We used ABC44-treated cell lysates as our positive control since ABC44 exhibiting potent PPT1 inhibition in HepG2 cells ( $\text{IC}_{50}$  1.26  $\mu\text{M}$ , Table 1) has been reported to be even more potent ( $\text{IC}_{50}$  0.1  $\mu\text{M}$  against recombinant PPT1).<sup>36</sup>

**Nanoscale Differential Scanning Fluorimetry.** We employed nanoDSF to determine the stability of PPT1 by monitoring the intrinsic fluorescence of tryptophan or tyrosine as a measure of its folding state.<sup>48</sup> We evaluated several of the

compounds reported in Figure 1 and additional small molecules that could potentially act as chaperones. We tested 18 compounds and identified 10 compounds that bind to and stabilize or destabilize PPT1 > 2  $^{\circ}\text{C}$  (Figure 3), such as rifapentine ( $\Delta T_m$  3.9  $^{\circ}\text{C}$ ), molsidomine ( $\Delta T_m$  2.1  $^{\circ}\text{C}$ ), tetracycline ( $\Delta T_m$  3.4  $^{\circ}\text{C}$ ), promethazine ( $\Delta T_m$  2.7  $^{\circ}\text{C}$ ), metronidazole ( $\Delta T_m$  2.5  $^{\circ}\text{C}$ ), deschloroclozapine ( $\Delta T_m$  3.0  $^{\circ}\text{C}$ ), carlgumic acid ( $\Delta T_m$  3.1  $^{\circ}\text{C}$ ), chlorpropamide ( $\Delta T_m$  3.4  $^{\circ}\text{C}$ ), amodiaquine ( $\Delta T_m$  3.3  $^{\circ}\text{C}$ ), and proguanil ( $\Delta T_m$  2.1  $^{\circ}\text{C}$ ).

**Microscale Thermophoresis.** We additionally developed a microscale thermophoresis (MST)<sup>49</sup> assay to determine the dissociation constant or  $K_d$  (Figure 4). We tested amodiaquine, proguanil, mefloquine, quinine, chlorpropamide, actinomycin D, and carlgumic acid to measure binding (Figure 4). Out of these molecules, amodiaquine showed the highest affinity for PPT1, with a  $K_d$  of 46 nM (Figure 3).

**Neuroblastoma SH-SY5Y Cell Line Inhibition.** Since PPT1 was described to be the target shared across monomeric and dimeric chloroquine derivatives in cancer,<sup>37</sup> and it is expressed in neuroblastoma, we have also evaluated chloroquine and other antimalarials that showed stabilization, binding, or inhibitory PPT1 activity in the neuroblastoma SH-SY5Y cell line. Amodiaquine inhibited neuroblastoma with an  $\text{IC}_{50}$  of 17  $\mu\text{M}$  (Figure 5A), mefloquine with an  $\text{IC}_{50}$  of 8  $\mu\text{M}$  (Figure 5B), chloroquine with an  $\text{IC}_{50}$  of 44  $\mu\text{M}$  (Figure 5C), and Lys05 with an  $\text{IC}_{50}$  of 9.5  $\mu\text{M}$  (Figure 5D). Hydroxychloroquine did not reach a 50% decrease in cell viability at the highest concentration tested (Figure S3).

**Machine Learning Model for PPT1.** The data from the screen for inhibition of PPT1 in vitro was used to build a Bayesian classification machine learning model with Assay Central (Figure S5) using our methods as described previously.<sup>50,51</sup> Compounds that showed a percentage of

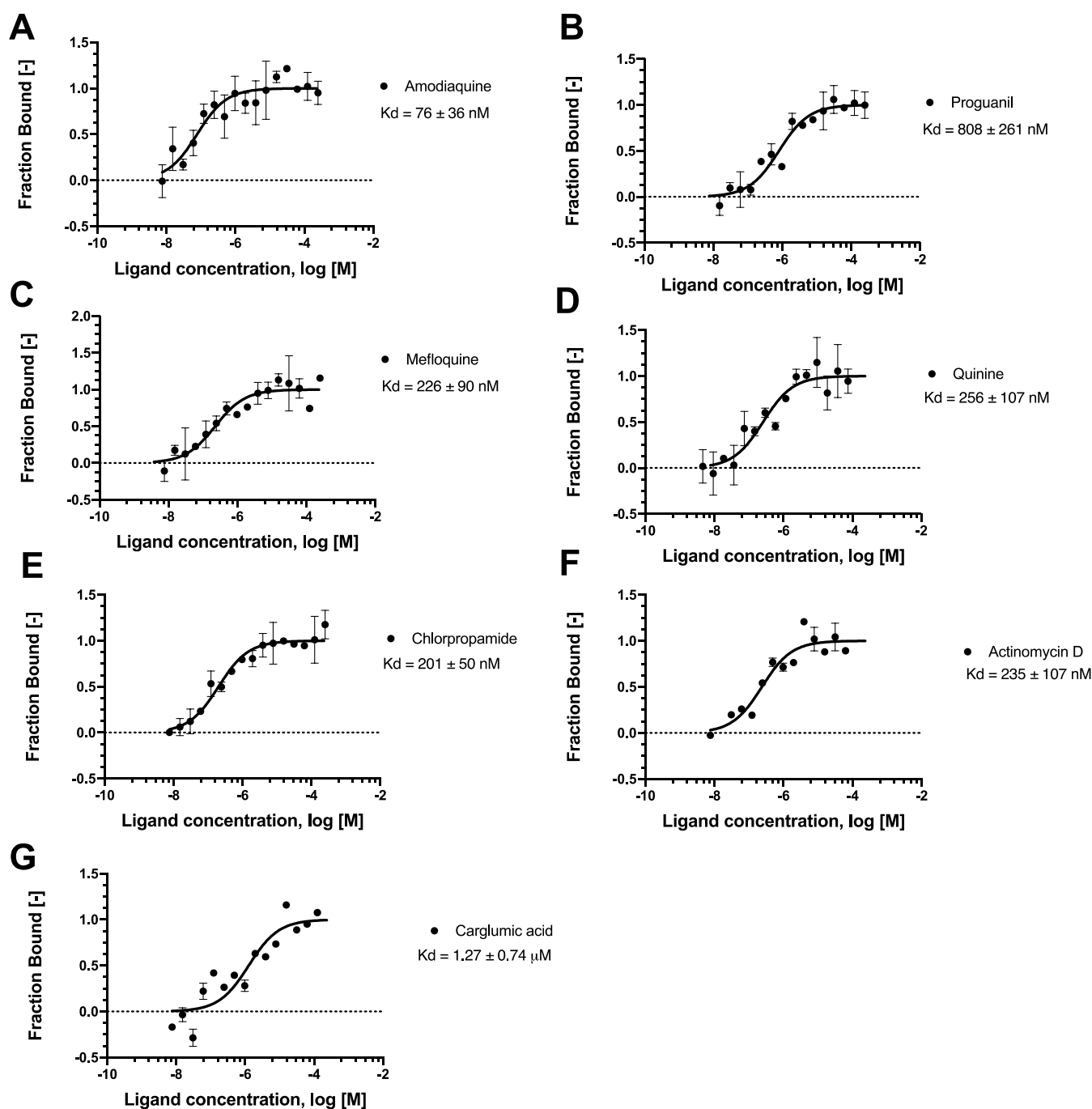


**Figure 4.** MST binding analysis for the interaction between PPT1 and compounds. (A) Amodiaquine, (B) proguanil, (C) mefloquine, (D) quinine, (E) chlorpropamide, (F) actinomycin D, and (G) carglumic acid. The concentration of labeled PPT1 RBD is kept constant at 5 nM, while the ligand concentration varies between 250  $\mu$ M and 7.63 nM. The serial titrations result in measurable changes in the fluorescence signal within a temperature gradient that can be used to calculate the dissociation constant. The curve is shown as fraction bound [-] against compound concentration on a log scale.

inhibition higher than 60% were considered active, and those below this were considered inactive. The model was built using ECFP6 fingerprints, and the fivefold cross-validation ROC was  $>0.7$ ; however, other statistics generated were poor likely due to the highly imbalanced data set (40 hits). This model was used for the virtual screening of several commercial libraries, yet it did not result in the identification of additional compounds.

## DISCUSSION

PPT1 is an understudied drug target for a rare disease,<sup>52</sup> and it has been recently described as having an important role in cancer<sup>37</sup> and other neurological diseases,<sup>8,53</sup> besides the PPT1 mutations described to cause CLN1 Batten disease.<sup>52</sup> In order to find novel molecules that bind or inhibit PPT1, we screened the MicroSource Spectrum Collection, which led to the identification of 40 compounds with activity  $>60\%$  when screened. We followed up 11 compounds with dose–response relationships (Figure 1A,B) and orlistat (Table 1 and Figure

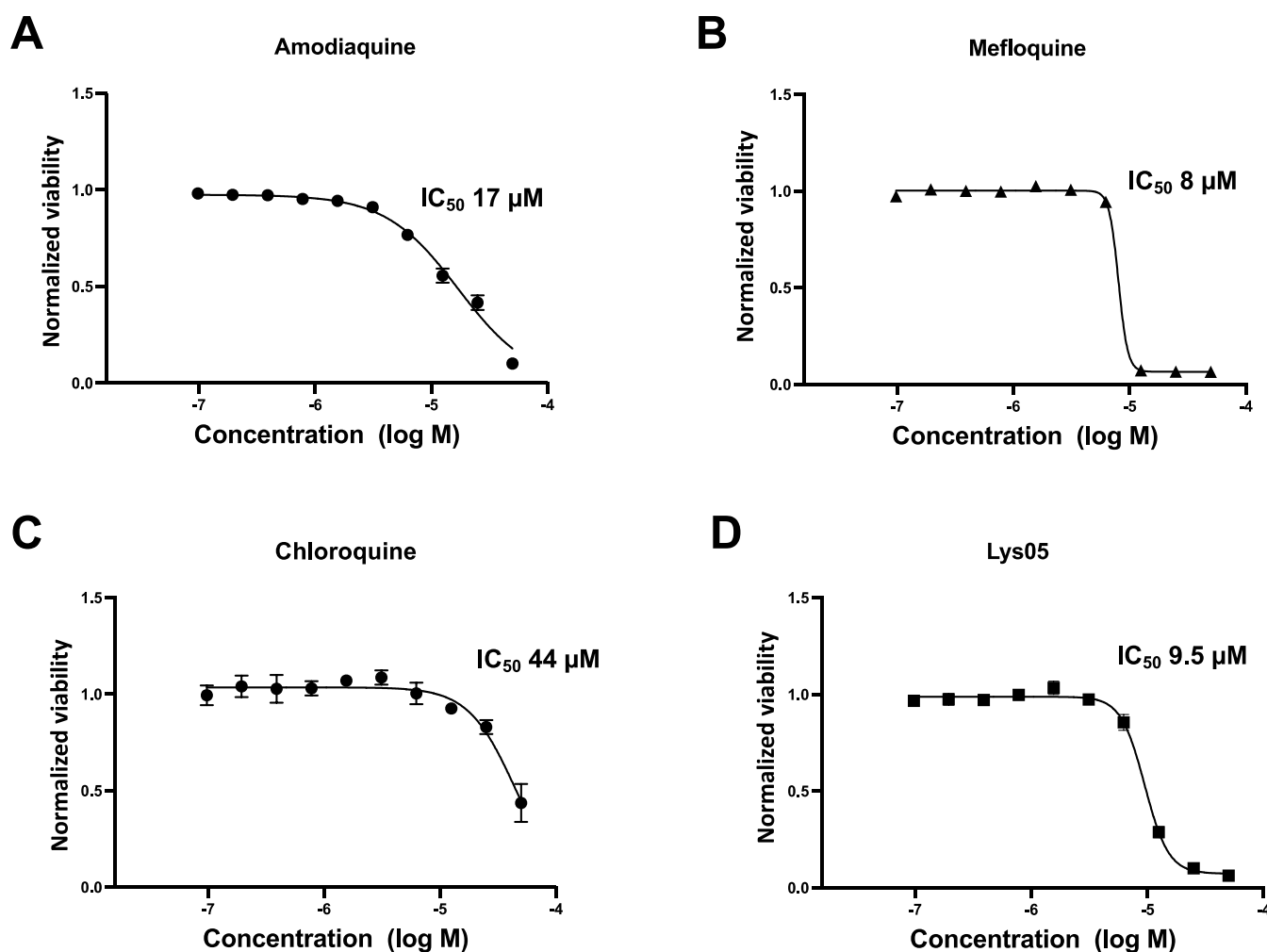


**Figure 5.** Compounds tested in the neuroblastoma SH-SY5Y cell line. (A) Amodiaquine, (B) mefloquine, (C) chloroquine, and (D) Lys05. Normalized viability was calculated after adjusting the effects of DMSO in vehicle-only controls, where 1 represents 100% cell viability and 0 represents 0% cell viability.

1D). Most of the compounds showed high  $IC_{50} > 100 \mu M$ ; however, orlistat showed an  $IC_{50}$  of 178.8 nM, an improvement on the previously described inhibitor ABC44 ( $IC_{50}$  1.2  $\mu M$ , Table 1), which is a PPT1 inhibitor in vitro and in vivo.<sup>36</sup> The orlistat  $IC_{50}$  also has a higher affinity for PPT1 than for the FASN.<sup>45</sup> We also tested the activity of a closely structurally related compound palmostatin B, which showed an  $IC_{50}$  of 11.8 nM (8.7–15.6 nM). To the best of our knowledge, orlistat and palmostatin B are the most potent PPT1 inhibitors that have been reported to date. We have also tested these compounds in cells (Figure 2A) and demonstrated that they have poor uptake likely due to their hydrophobic nature (Figure 2B).

In the past decade, the importance of protein palmitoylation in tumorigenesis has become evident. It plays a crucial role in various critical aspects of cancer, such as cell proliferation and survival, cell invasion and metastasis, as well as the modulation of antitumor immune responses.<sup>54</sup> We have reported here that orlistat and palmostatin B are nanomolar inhibitors of PPT1 which are structurally related using Tanimoto similarity (MACCS fingerprints) of 0.65, and both molecules contain a hydrophobic tail and a  $\beta$  lactone ring. Orlistat is approved in several countries including the US for the treatment of obesity, as it can prevent absorption of lipids through binding

covalently to the active serine residues of pancreatic lipase.<sup>55</sup> A limitation of this molecule is that it is poorly orally absorbed which may necessitate structural modification, nanoformulation, or other techniques to improve cell entry.<sup>56</sup> Orlistat has been investigated for several cancer types, such as prostate, colorectal, and hepatoma cells as it is known to inhibit FASN, an enzyme linked with tumor progression.<sup>44,57–59</sup> Our discovery that orlistat can also inhibit PPT1 with nanomolar activity in vitro shows a potential new mechanism of action since PPT1 is known to be significantly overexpressed in several cancer types, including breast, thyroid, and gastric cancers.<sup>37</sup> Higher expression levels of PPT1 in tumors have also been correlated with shorter overall survival across various cancer types, including head and neck, esophageal, and renal cell cancers.<sup>37</sup> Orlistat has previously been shown to inhibit FASN ( $IC_{50}$  1.35  $\mu M$ );<sup>45</sup> however, the  $IC_{50}$  value to inhibit cancer cell growth through FASN inhibition range is much higher (from 5 to 40  $\mu M$ ) in T-cell leukemia and prostate cancer cell lines,<sup>44,60</sup> which confirms our finding that poor cell penetration is likely a reason for poor PPT1 inhibition in cells by orlistat necessitating improved formulation to increase cellular potency.

Palmostatin B is a nonspecific depalmitoylation inhibitor that primarily inhibits the acyl-protein thioesterases APT-1 and

APT-2,<sup>46</sup> which, like PPT1, can catalyze the removal of S-palmitoylation from protein substrates.<sup>54</sup> It was earlier demonstrated that the combination of palmotatin B with the FLT3 inhibitor gilteritinib significantly suppressed FLT3-ITD-mediated signaling and leukemia progression.<sup>61</sup> We are not aware of the absorption of palmotatin being studied, but it is likely also to be poor due to its similarity to orlistat. Both orlistat and palmotatin B contain a  $\beta$ -lactone warhead which is known to react and inhibit enzymes from the serine or threonine hydrolase class.<sup>45,62</sup>

PPT1 was previously described to be the target of chloroquine and derivatives in neuroblastoma.<sup>37</sup> High PPT1 expression predicts poor clinical outcome while the PPT1 inhibitor DC661 enhanced sorafenib sensitivity in hepatocellular carcinoma.<sup>63</sup> We therefore determined the enzyme activity of PPT1 in the presence of several antimalarial drugs (Figure 1C and Table S3). From the compounds tested, we showed that the antimalarial amodiaquine inhibits PPT1 with an  $IC_{50}$  of 344  $\mu$ M and binds to this enzyme with a  $K_d$  of 76 nM and also increased the  $\Delta T_m$  of 3.3  $^{\circ}$ C (Figure 3D). Chloroquine and hydroxychloroquine were shown to inhibit PPT1 activity in neuroblastoma cancer cell lines,<sup>37</sup> with an  $IC_{50}$  of 47.2  $\mu$ M for chloroquine and  $IC_{50}$  of 109.1  $\mu$ M for hydroxychloroquine; however, they did not show significant changes in the  $\Delta T_m$  (Figure 3D). For comparison, we also evaluated the enzymatic activity in the presence of the inhibitor DC661, which was previously described to be more potent against PPT1<sup>37</sup> than chloroquine and hydroxychloroquine, and in our assay, DC661 showed an estimated  $IC_{50}$  of 129.6  $\mu$ M. The  $IC_{50}$  values using purified PPT1 measured for chloroquine and DC661 are therefore the same order of magnitude as previously reported. These compounds are all lysosomotropic and their inhibition of PPT1 in cancer cell lines could potentially rely more on their capacity to accumulate in the lysosomes<sup>64,65</sup> than their individual in vitro inhibition against the purified PPT1.

Pharmacological chaperones can be active site-specific inhibitors or allosteric molecules that stabilize the conformation of the mutant protein in order to increase the level of the residual activity to reverse the clinical phenotype.<sup>10</sup> Finding such small molecule modulators may have an impact on the quality of life and increase the lifespan of CLN1 patients. Currently, as no therapy has received regulatory approval and, therefore, none is clinically available to reverse the neurological decline in CLN1 Batten disease or potentially restore PPT1 activity, efforts have been focused on gene therapy and enzyme replacement as with most other LSDs.<sup>14,15</sup> To date, the only molecule reported to act as a chaperone for PPT1 is a peptide combined with palmitate that was demonstrated to cause a twofold increase in PPT1, using cell lines T75P/R151X.<sup>17</sup> Here, we reported 10 molecules that can increase PPT1 stability  $\Delta T_m > 2$   $^{\circ}$ C (Figure 3) using nanoDSF. Among them is rifapentine with a  $\Delta T_m$  of 3.9  $^{\circ}$ C, tetracycline with a  $\Delta T_m$  of 3.4  $^{\circ}$ C, and deschloroclozapine with a  $\Delta T_m$  of 3.0  $^{\circ}$ C. These molecules could be tested in CLN1 patient cell lines in future to verify if they could rescue enzyme activity. Of these, deschloroclozapine is perhaps the most interesting because it can also cross the BBB.<sup>66</sup>

PPT1 represents a new target in cancer, and we have reported more potent inhibitors that could be evaluated for other types of cancer (Figure 4). PPT1 expression approached the upper limits of RNA expression across multiple tumor types in the Broad Novartis Cancer Cell Line Encyclopedia

(<https://portals.broadinstitute.org/ccle>). In The Cancer Genome Atlas (TCGA) database, PPT1 gene amplification is present in 4–10% of ovarian, esophageal, bladder, uterine, and stomach cancers and PPT1 expression was significantly higher in metastases compared to primary melanoma tumors.<sup>37</sup> PPT1 was also associated with shorter overall survival in a variety of cancers including esophageal cancer, head and neck cancer, renal cell carcinoma, and hepatocellular cancer.<sup>37</sup>

There are no large data sets available in the public domain (ChEMBL and PubChem) describing compounds that could bind or inhibit PPT1. We have now performed a large screening which identified a few inhibitors, and this is problematic for attempts at machine learning because of the high data set imbalance. Although we could build a classification model with reasonable fivefold cross-validation statistics (Figure S4), this model was not successful in identifying additional PPT1 inhibitors. The use of alternative machine learning algorithms and thresholds was attempted and also unsuccessful. It is likely that in order to improve our machine learning model further, we would need to generate a much larger data set or use other specialized algorithms that could deal with smaller data sets such as few-shot learning.<sup>67</sup>

We have employed several in vitro screening and biophysical techniques as well as a machine learning model in an effort to find potential molecules for PPT1 and this type of approach may aid research not only for small molecule modulators or chaperones for CLN1 Batten disease but also for broader therapeutic uses in neurodegeneration and cancer. Understanding the role of PPT1 depalmitoylase is a fertile area for basic science and translational research,<sup>20,54</sup> and the compounds described here could further help to advance research in the field. Here, we report the repurposing as well as discovery and characterization of new compounds that inhibit or stabilize PPT1, and among them, identification of the most potent PPT1 inhibitors in vitro, namely, orlistat and palmotatin B. This sheds light on the mechanism of action of these compounds and opens new doors for exploring them as potential treatments for cancer and other neurological diseases by targeting PPT1. We also highlight the limitations of these compounds as, clearly due to their high hydrophobicity, they have poor cellular penetration which would require evaluation of other formulation methods.<sup>56</sup>

## METHODS

**Compounds.** Compounds were purchased from MedChemExpress (MCE, Monmouth Junction, NJ). Palmotatin B was purchased from Sigma-Aldrich. The MicroSource Spectrum screening compound library (MicroSource Discovery Systems, Inc., Gaylordsville, CT, USA) was a generous gift from Dr. Ethan Perlstein (Perlara). PPT1 was obtained from Dr. Sandra L. Hofmann (University of Texas Southwestern Medical Center).

**High-Throughput Screening.** PPT1 was purified and the activity was quantified as previously described.<sup>42,68</sup> Briefly, palmitate linked to 4-methylumbelliferyl-6-thio- $\beta$ -D-glucopyranoside (MU-6S-Palm- $\beta$ Glc) was used as a synthetic substrate. Thioester bond cleavage by PPT1 released palmitate and the intermediate 4-methylumbelliferyl-6-thio- $\beta$ -D-glucopyranoside. This intermediate was further hydrolyzed to 4-methylumbelliferone, via exogenous almond  $\beta$ -glucosidase, and its fluorescence was measured as a means of quantifying the PPT1 cleavage of palmitate groups. For dose–response curves, compounds (twofold serial dilutions, 10 points) were

incubated 10 to 20 min at room temperature with PPT1 prior to the addition of the substrate. Fluorescence was measured at the following wavelengths: Ex 365 nm and Em 448 nm using the plate reader SpectraMax iD5 (Molecular Devices). Percent inhibition was calculated on a scale of 0% (i.e., activity with DMSO vehicle only) to 100% (no enzyme added). For dose–response curves,  $IC_{50}$  values were reported with a 95% confidence interval (95% CI).

**Nanoscale Differential Scanning Fluorimetry.** PPT1 was diluted to 5  $\mu$ M in PBS at pH 7.4 containing 1 mM  $\beta$ -mercaptoethanol and incubated with 50  $\mu$ M of each compound at 4 °C for 1 h. NanoDSF experiments were performed as described<sup>69</sup> using Prometheus NT.48 (NanoTemper). The fluorescence ratio at 330/350 nm wavelength is reported for all nanoDSF experiments.

**Microscale Thermophoresis.** Microscale thermophoresis (MST) was performed as previously described<sup>70</sup> using the Monolith NT.115 (NanoTemper). MST buffer contained HEPES 10 mM, pH 7.4, NaCl 150 mM, 1 mM  $\beta$ -mercaptoethanol, and 0.2% Triton X-100.

**Testing Compounds in the Neuroblastoma SH-SY5Y Cell Line.** NB cell lines (SH-SY5Y) were plated (4000 cells/well) in 45  $\mu$ L of fresh media in 384-well plates and treated with 5  $\mu$ L of increasing concentrations of the compound. Plates were incubated at 37 °C with 5% CO<sub>2</sub> for 48 h and the cytotoxic effect was measured after the addition of alamarBlue for 18 h. All cell lines were cultured in DMEM/F12 medium (Gibco, Life Technologies, NY, USA) containing 10% fetal bovine serum (Seradigm, VWR, USA). Drugs were added in quadruplicate wells using a Tecan EVO150 with a 96 MCA head (Tecan Group Ltd., Switzerland). Each plate included controls for drug solvation effects from DMSO. Fluorescence intensity was measured using an excitation filter of 535 nm and an emission filter of 595 nm on an Infinite F200 microplate reader with a Connect Stacker (Tecan Group Ltd.) using iControl software (version 1.12). The resulting relative fluorescence units are proportional to the cellular redox activity, which is a common proxy for the quantity of living cells. Percent viabilities were calculated after adjustment of the effects of DMSO in vehicle-only controls. Each experiment was repeated for a total of 2–7 biological replicates and estimated  $IC_{50}$ 's and maximal effects were combined using geometric and arithmetic means, respectively.

**Cell Line Overexpressing PPT1 Testing.** HepG2 cells were obtained from ATCC and were cultured in Dulbecco's modified Eagle medium + 10% FBS at 37 °C calcium and 5% CO<sub>2</sub> level. To test PPT1 inhibition in cells, HepG2 cells were seeded in 6-well plates and left overnight to adhere. The following day, compounds were added to cell culture media and incubated for 5 h, followed by cell lysis and protein extraction. The MPER extraction agent (Thermo Fisher Scientific) along with the Halt protease inhibitor (Thermo Fisher Scientific) in 0.5% Triton X100 were used for cell lysis followed by centrifugation at 14,000 rpm for 15 min to obtain cell lysates. Lysates were normalized for protein amount and 5  $\mu$ L of cell lysates were used for the PPT1 assay as described earlier with modifications.<sup>42,47</sup> 4-methylumbelliferone (4-MU) (Sigma-Aldrich) was used to make a standard curve. Fluorescence intensity was measured using a SpectraMax iD5 plate reader (Molecular Devices). For testing PPT1 inhibitor activity in cell lysates, 50  $\mu$ L of HepG2 cell lysates were treated with the compounds for an hour, followed by enzyme inhibition using the PPT1 enzyme assay as above. Experiments

were performed in biological duplicates containing technical replicates in triplicates. The percent PPT1 activity was determined relative to that of the DMSO control.

**Machine Learning.** Our in-house software Assay Central<sup>71,72</sup> was used to curate our screening data. The interpretation of the metrics, as well as the prediction and applicability scores, has been described previously.<sup>50,51,71,73,74</sup> While Assay Central can select a reasonable threshold, a threshold of 60% inhibition was set for the models. Compounds with a percent inhibition higher than this threshold were considered active and those below were considered inactive. Any ambiguous metal complexes or mixtures of compounds were removed from the training set to increase the performance of the models. We generated a Bayesian model as previously described using our Assay Central software using ECFP6 descriptors.<sup>75,76</sup> Each model in Assay Central includes the following metrics for evaluative predictive performance: Recall, Precision, Specificity, F1-Score, ROC curve, Cohen's Kappa (CK),<sup>77,78</sup> and the Matthews Correlation Coefficient (MCC).<sup>79</sup>

## ■ ASSOCIATED CONTENT

### Supporting Information

The Supporting Information is available free of charge at <https://pubs.acs.org/doi/10.1021/acsomega.3c09607>.

$K_m$  determination for PPT1, dose–response curves for vanillin and rutin against PPT1, compounds tested in neuroblastoma cell lines, PPT1 inhibition in HepG2 cells and cell extracts, PPT1 inhibition machine learning model statistics, summary of small molecule PCT products approved or in clinical trials, percent inhibition of the top hits from the Spectrum Collection library screened against PPT1, percent inhibition of antimalarials, natural products and other compounds tested against PPT1, and supplemental references (PDF)

## ■ AUTHOR INFORMATION

### Corresponding Author

Sean Ekins – Collaborations Pharmaceuticals, Inc., Raleigh, North Carolina 27606, United States; [orcid.org/0000-0002-5691-5790](https://orcid.org/0000-0002-5691-5790); Email: [sean@collaborationspharma.com](mailto:sean@collaborationspharma.com)

### Authors

Ana C. Puhl – Collaborations Pharmaceuticals, Inc., Raleigh, North Carolina 27606, United States

Renuka Raman – Collaborations Pharmaceuticals, Inc., Raleigh, North Carolina 27606, United States

Tammy M. Havener – UNC Catalyst for Rare Diseases, Eshelman School of Pharmacy, University of North Carolina at Chapel Hill, Chapel Hill, North Carolina 27599, United States; Present Address: Structural Genomics Consortium and Division of Chemical Biology and Medicinal Chemistry, Eshelman School of Pharmacy, University of North Carolina at Chapel Hill, Chapel Hill, North Carolina, 27599, United States of America; [orcid.org/0000-0002-4613-0498](https://orcid.org/0000-0002-4613-0498)

Eni Minerali – Collaborations Pharmaceuticals, Inc., Raleigh, North Carolina 27606, United States

Anthony J. Hickey – UNC Catalyst for Rare Diseases, Eshelman School of Pharmacy, University of North Carolina at Chapel Hill, Chapel Hill, North Carolina 27599, United States

States; RTI International, Research Triangle Park, North Carolina 27709, United States

Complete contact information is available at:  
<https://pubs.acs.org/10.1021/acsomega.3c09607>

### Author Contributions

A.C.P. and S.E. drafted the manuscript and all authors read and accepted the manuscript.

### Funding

We kindly acknowledge NIH funding: R44GM122196-02A1 from NIGMS; 1R43NS107079-01, 3R43NS107079-01S1, 3R43NS107079-01S2, and 5R44NS107079-03 from NIH/NINDS; and 1R43AT010585-01 from NCCIH.

### Notes

The authors declare the following competing financial interest(s): S.E. is the owner and A.C.P., R.R., and E.M. are employees of Collaborations Pharmaceuticals, Inc.

## ACKNOWLEDGMENTS

The authors would like to kindly acknowledge contributions from Kimberley Zorn, Dr. Patricia Vignaux, Dr. Thomas Lane, Jennifer Klein, Dr. Edward Anderson and Dr. Alex Clark. We also thank Dr. Sandra Hofmann, Dr. Jonathan Cooper, and Dr. Mark Sands for providing the PPT1 enzyme and discussion.

## ABBREVIATIONS

4-MU, 4-methylumbelliferyl; BBB, blood–brain barrier; CNS, central nervous system; FASN, fatty acid synthase; GAD65, glutamic acid decarboxylase 65; GFAP, glial fibrillary acidic protein; HTS, high-throughput screening; LSD, lysosomal storage disease; CLN1 disease, infantile neuronal ceroid lipofuscinosis; MST, microscale thermophoresis; nanoDSE, nanoscale differential scanning fluorimetry; NMDAR, N-methyl-D-aspartate receptor; PPT1, palmitoyl-protein thioesterase 1; PCT, pharmacological chaperone therapy; TCGA, The Cancer Genome Atlas

## REFERENCES

- (1) Ballabio, A.; Gieselmann, V. Lysosomal disorders: from storage to cellular damage. *Biochim. Biophys. Acta* **2009**, *1793* (4), 684–696.
- (2) Karageorgos, L. E.; Isaac, E. L.; Brooks, D. A.; Ravenscroft, E. M.; Davey, R.; Hopwood, J. J.; Meikle, P. J. Lysosomal biogenesis in lysosomal storage disorders. *Exp. Cell Res.* **1997**, *234* (1), 85–97.
- (3) Platt, F. M. Emptying the stores: lysosomal diseases and therapeutic strategies. *Nat. Rev. Drug Discovery* **2018**, *17* (2), 133–150.
- (4) Atiskova, Y.; Bartsch, S.; Danyukova, T.; Becker, E.; Hagel, C.; Storch, S.; Bartsch, U. Mice deficient in the lysosomal enzyme palmitoyl-protein thioesterase 1 (PPT1) display a complex retinal phenotype. *Sci. Rep.* **2019**, *9* (1), 14185.
- (5) Miller, J. N.; Kovacs, A. D.; Pearce, D. A. The novel Cln1 (R151X) mouse model of infantile neuronal ceroid lipofuscinosis (INCL) for testing nonsense suppression therapy. *Hum. Mol. Genet.* **2015**, *24* (1), 185–196.
- (6) Johnson, T. B.; Cain, J. T.; White, K. A.; Ramirez-Montealegre, D.; Pearce, D. A.; Weimer, J. M. Therapeutic landscape for Batten disease: current treatments and future prospects. *Nat. Rev. Neurol.* **2019**, *15* (3), 161–178.
- (7) Finn, R.; Kovacs, A. D.; Pearce, D. A. Treatment of the Ppt1(–/–) mouse model of infantile neuronal ceroid lipofuscinosis with the N-methyl-D-aspartate (NMDA) receptor antagonist memantine. *J. Child Neurol.* **2013**, *28* (9), 1159–1168.
- (8) Koster, K. P.; Francesconi, W.; Berton, F.; Alahmadi, S.; Srinivas, R.; Yoshii, A. Developmental NMDA receptor dysregulation in the

infantile neuronal ceroid lipofuscinosis mouse model. *Elife* **2019**, *8*, No. e40316.

(9) Boyd, R. E.; Lee, G.; Rybczynski, P.; Benjamin, E. R.; Khanna, R.; Wustman, B. A.; Valenzano, K. J. Pharmacological chaperones as therapeutics for lysosomal storage diseases. *J. Med. Chem.* **2013**, *56* (7), 2705–2725.

(10) Parenti, G. Treating lysosomal storage diseases with pharmacological chaperones: from concept to clinics. *EMBO Mol. Med.* **2009**, *1* (5), 268–279.

(11) Fan, J. Q. A counterintuitive approach to treat enzyme deficiencies: use of enzyme inhibitors for restoring mutant enzyme activity. *Biol. Chem.* **2008**, *389* (1), 1–11.

(12) Zheng, W.; Padia, J.; Urban, D. J.; Jadhav, A.; Goker-Alpan, O.; Simeonov, A.; Goldin, E.; Auld, D.; LaMarca, M. E.; Inglese, J.; Austin, C. P.; Sidransky, E. Three classes of glucocerebrosidase inhibitors identified by quantitative high-throughput screening are chaperone leads for Gaucher disease. *Proc. Natl. Acad. Sci. U.S.A.* **2007**, *104* (32), 13192–13197.

(13) Almeciga-Diaz, C. J.; Hidalgo, O. A.; Olarte-Avellaneda, S.; Rodriguez-Lopez, A.; Guzman, E.; Garzon, R.; Pimentel-Vera, L. N.; Puentes-Tellez, M. A.; Rojas-Rodriguez, A. F.; Gorshkov, K.; Li, R.; Zheng, W. Identification of Ezetimibe and Pranlukast as Pharmacological Chaperones for the Treatment of the Rare Disease Mucopolysaccharidosis Type IVA. *J. Med. Chem.* **2019**, *62* (13), 6175–6189.

(14) Valenzano, K. J.; Khanna, R.; Powe, A. C.; Boyd, R.; Lee, G.; Flanagan, J. J.; Benjamin, E. R. Identification and characterization of pharmacological chaperones to correct enzyme deficiencies in lysosomal storage disorders. *Assay Drug Dev. Technol.* **2011**, *9* (3), 213–235.

(15) Suzuki, Y. Emerging novel concept of chaperone therapies for protein misfolding diseases. *Proc. Jpn. Acad. Ser. B Phys. Biol. Sci.* **2014**, *90* (5), 145–162.

(16) Beck, M. Treatment strategies for lysosomal storage disorders. *Dev. Med. Child Neurol.* **2018**, *60* (1), 13–18.

(17) Dawson, G.; Schroeder, C.; Dawson, P. E. Palmitoyl:protein thioesterase (PPT1) inhibitors can act as pharmacological chaperones in infantile Batten disease. *Biochem. Biophys. Res. Commun.* **2010**, *395* (1), 66–69.

(18) Hellsten, E.; Vesa, J.; Olkkonen, V. M.; Jalanko, A.; Peltonen, L. Human palmitoyl protein thioesterase: evidence for lysosomal targeting of the enzyme and disturbed cellular routing in infantile neuronal ceroid lipofuscinosis. *EMBO J.* **1996**, *15* (19), S240–S245.

(19) Naumenko, V. S.; Ponimaskin, E. Palmitoylation as a Functional Regulator of Neurotransmitter Receptors. *Neural Plast.* **2018**, *2018*, 1–18.

(20) Koster, K. P.; Yoshii, A. Depalmitoylation by Palmitoyl-Protein Thioesterase 1 in Neuronal Health and Degeneration. *Front. Synaptic Neurosci.* **2019**, *11*, 25.

(21) Biesemann, C.; Grønborg, M.; Luquet, E.; Wichert, S. P.; Bernard, V.; Bungers, S. R.; Cooper, B.; Varoqueaux, F.; Li, L.; Byrne, J. A.; Urlaub, H.; Jahn, O.; Brose, N.; Herzog, E. Proteomic screening of glutamatergic mouse brain synaptosomes isolated by fluorescence activated sorting. *EMBO J.* **2014**, *33* (2), 157–170.

(22) Gonzalez-Lozano, M. A.; Klemmer, P.; Gebuis, T.; Hassan, C.; van Nierop, P.; van Kesteren, R. E.; Smit, A. B.; Li, K. W. Dynamics of the mouse brain cortical synaptic proteome during postnatal brain development. *Sci. Rep.* **2016**, *6*, 35456.

(23) Velásquez, E.; Nogueira, F. C. S.; Velásquez, I.; Schmitt, A.; Falkai, P.; Domont, G. B.; Martins-de-Souza, D. Synaptosomal Proteome of the Orbitofrontal Cortex from Schizophrenia Patients Using Quantitative Label-Free and iTRAQ-Based Shotgun Proteomics. *J. Proteome Res.* **2017**, *16* (12), 4481–4494.

(24) El-Husseini, A. E. D.; Bredt, D. S. Protein palmitoylation: a regulator of neuronal development and function. *Nat. Rev. Neurosci.* **2002**, *3* (10), 791–802.

(25) Fukata, Y.; Dimitrov, A.; Boncompain, G.; Vielemeyer, O.; Perez, F.; Fukata, M. Local palmitoylation cycles define activity-

- regulated postsynaptic subdomains. *J. Cell Biol.* **2013**, *202* (1), 145–161.
- (26) Gorenberg, E. L.; Massaro Tiede, S.; Yucel, B.; Zhao, H. R.; Chou, V.; Wirak, G. S.; Tomita, S.; Lam, T. T.; Chandra, S. S. Identification of substrates of palmitoyl protein thioesterase 1 highlights roles of depalmitoylation in disulfide bond formation and synaptic function. *PLoS Biol.* **2022**, *20* (3), No. e3001590.
- (27) Yuan, W.; Lu, L.; Rao, M.; Huang, Y.; Liu, C. E.; Liu, S.; Zhao, Y.; Liu, H.; Zhu, J.; Chao, T.; Wu, C.; Ren, J.; Lv, L.; Li, W.; Qi, S.; Liang, Y.; Yue, S.; Gao, J.; Zhang, Z.; Kong, E. GFAP hyperpalmitoylation exacerbates astrogliosis and neurodegenerative pathology in PPT1-deficient mice. *Proc. Natl. Acad. Sci. U.S.A.* **2021**, *118* (13), No. e2022261118.
- (28) Lyly, A.; Marjavaara, S. K.; Kytälä, A.; Uusi-Rauva, K.; Luiro, K.; Kopra, O.; Martinez, L. O.; Tanhuanpää, K.; Kalkkinen, N.; Suomalainen, A.; Jauhainen, M.; Jalanko, A. Deficiency of the INCL protein Ppt1 results in changes in ectopic F1-ATP synthase and altered cholesterol metabolism. *Hum. Mol. Genet.* **2008**, *17* (10), 1406–1417.
- (29) Bagh, M. B.; Peng, S.; Chandra, G.; Zhang, Z.; Singh, S. P.; Pattabiraman, N.; Liu, A.; Mukherjee, A. B. Misrouting of v-ATPase subunit V0a1 dysregulates lysosomal acidification in a neurodegenerative lysosomal storage disease model. *Nat. Commun.* **2017**, *8*, 14612.
- (30) Rebecca, V. W.; Nicastrì, M. C.; McLaughlin, N.; Fennelly, C.; McAfee, Q.; Ronghe, A.; Nofal, M.; Lim, C. Y.; Witze, E.; Chude, C. I.; Zhang, G.; Alicea, G. M.; Piao, S.; Murugan, S.; Ojha, R.; Levi, S. M.; Wei, Z.; Barber-Rotenberg, J. S.; Murphy, M. E.; Mills, G. B.; Lu, Y.; Rabinowitz, J.; Marmorstein, R.; Liu, Q.; Liu, S.; Xu, X.; Herlyn, M.; Zoncu, R.; Brady, D. C.; Speicher, D. W.; Winkler, J. D.; Amaravadi, R. K. A Unified Approach to Targeting the Lysosome's Degradative and Growth Signaling Roles. *Cancer Discov.* **2017**, *7* (11), 1266–1283.
- (31) Sapir, T.; Segal, M.; Grigoryan, G.; Hansson, K. M.; James, P.; Segal, M.; Reiner, O. The Interactome of Palmitoyl-Protein Thioesterase 1 (PPT1) Affects Neuronal Morphology and Function. *Front. Cell. Neurosci.* **2019**, *13*, 92.
- (32) Lee, G.; Thangavel, R.; Sharma, V. M.; Litersky, J. M.; Bhaskar, K.; Fang, S. M.; Do, L. H.; Andreadis, A.; Van Hoesen, G.; Ksiezak-Reding, H. Phosphorylation of tau by fyn: implications for Alzheimer's disease. *J. Neurosci.* **2004**, *24* (9), 2304–2312.
- (33) Kanaani, J.; Patterson, G.; Schaufele, F.; Lippincott-Schwartz, J.; Baekkeskov, S. A palmitoylation cycle dynamically regulates partitioning of the GABA-synthesizing enzyme GAD65 between ER-Golgi and post-Golgi membranes. *J. Cell Sci.* **2008**, *121* (4), 437–449.
- (34) Kim, S. J.; Zhang, Z.; Sarkar, C.; Tsai, P. C.; Lee, Y. C.; Dye, L.; Mukherjee, A. B. Palmitoyl protein thioesterase-1 deficiency impairs synaptic vesicle recycling at nerve terminals, contributing to neuropathology in humans and mice. *J. Clin. Invest.* **2008**, *118* (9), 3075–3086.
- (35) Kinarivala, N.; Trippier, P. C. Progress in the Development of Small Molecule Therapeutics for the Treatment of Neuronal Ceroid Lipofuscinoses (NCLs). *J. Med. Chem.* **2016**, *59* (10), 4415–4427.
- (36) Cognetta, A. B.; Niphakis, M. J.; Lee, H. C.; Martini, M. L.; Hulce, J. J.; Cravatt, B. F. Selective N-Hydroxyhydantoin Carbamate Inhibitors of Mammalian Serine Hydrolases. *Chem. Biol.* **2015**, *22* (7), 928–937.
- (37) Rebecca, V. W.; Nicastrì, M. C.; Fennelly, C.; Chude, C. I.; Barber-Rotenberg, J. S.; Ronghe, A.; McAfee, Q.; McLaughlin, N. P.; Zhang, G.; Goldman, A. R.; Ojha, R.; Piao, S.; Noguera-Ortega, E.; Martorella, A.; Alicea, G. M.; Lee, J. J.; Schuchter, L. M.; Xu, X.; Herlyn, M.; Marmorstein, R.; Gimotty, P. A.; Speicher, D. W.; Winkler, J. D.; Amaravadi, R. K. PPT1 Promotes Tumor Growth and Is the Molecular Target of Chloroquine Derivatives in Cancer. *Cancer Discov.* **2019**, *9* (2), 220–229.
- (38) Scifo, E.; Szwajda, A.; Soliymani, R.; Pezzini, F.; Bianchi, M.; Dapkunas, A.; Debski, J.; Uusi-Rauva, K.; Dadlez, M.; Gingras, A. C.; Tyynelä, J.; Simonati, A.; Jalanko, A.; Baumann, M. H.; Lalowski, M. Proteomic analysis of the palmitoyl protein thioesterase 1 interactome in SH-SY5Y human neuroblastoma cells. *J. Proteomics* **2015**, *123*, 42–53.
- (39) Cho, S.; Dawson, G. Palmitoyl protein thioesterase 1 protects against apoptosis mediated by Ras-Akt-caspase pathway in neuroblastoma cells. *J. Neurochem.* **2000**, *74* (4), 1478–1488.
- (40) Dawson, G.; Dawson, S. A.; Marinzi, C.; Dawson, P. E. Antitumor promoting effects of palmitoyl: protein thioesterase inhibitors against a human neurotumor cell line. *Cancer Lett.* **2002**, *187* (1–2), 163–168.
- (41) Cho, S.; Dawson, P. E.; Dawson, G. Antisense palmitoyl protein thioesterase 1 (PPT1) treatment inhibits PPT1 activity and increases cell death in LA-N-5 neuroblastoma cells. *J. Neurosci. Res.* **2000**, *62* (2), 234–240.
- (42) van Diggelen, O. P.; Keulemans, J. L.; Winchester, B.; Hofman, I. L.; Vanhanen, S. L.; Santavuori, P.; Voznyi, Y. V. A rapid fluorogenic palmitoyl-protein thioesterase assay: pre- and postnatal diagnosis of INCL. *Mol. Genet. Metab.* **1999**, *66* (4), 240–244.
- (43) Forsberg, M.; Lehtonen, M.; Heikkinen, M.; Savolainen, J.; Järvinen, T.; Männistö, P. T. Pharmacokinetics and pharmacodynamics of entacapone and tolcapone after acute and repeated administration: a comparative study in the rat. *J. Pharmacol. Exp. Ther.* **2003**, *304* (2), 498–506.
- (44) Kridel, S. J.; Axelrod, F.; Rozenkrantz, N.; Smith, J. W. Orlistat is a novel inhibitor of fatty acid synthase with antitumor activity. *Cancer Res.* **2004**, *64* (6), 2070–2075.
- (45) Richardson, R. D.; Ma, G.; Oyola, Y.; Zancanella, M.; Knowles, L. M.; Cieplak, P.; Romo, D.; Smith, J. W. Synthesis of Novel  $\beta$ -Lactone Inhibitors of Fatty Acid Synthase. *J. Med. Chem.* **2008**, *51* (17), 5285–5296.
- (46) Rusch, M.; Zimmermann, T. J.; Bürger, M.; Dekker, F. J.; Görmer, K.; Triola, G.; Brockmeyer, A.; Janning, P.; Böttcher, T.; Sieber, S. A.; Vetter, I. R.; Hedberg, C.; Waldmann, H. Identification of acyl protein thioesterases 1 and 2 as the cellular targets of the Ras-signaling modulators palmostatin B and M. *Angew. Chem., Int. Ed. Engl.* **2011**, *50* (42), 9838–9842.
- (47) Brun, S.; Bestion, E.; Raymond, E.; Bassissi, F.; Jilkova, Z. M.; Mezouar, S.; Rachid, M.; Novello, M.; Tracz, J.; Hamai, A.; Lalmanach, G.; Vanderlynden, L.; Legouffe, R.; Stauber, J.; Schubert, T.; Plach, M. G.; Courcambeck, J.; Drouot, C.; Jacquemot, G.; Serdjebi, C.; Roth, G.; Baudoin, J. P.; Ansaldi, C.; Decaens, T.; Halfon, P. GNS561, a clinical-stage PPT1 inhibitor, is efficient against hepatocellular carcinoma via modulation of lysosomal functions. *Autophagy* **2022**, *18* (3), 678–694.
- (48) Magnusson, A. O.; Szekrenyi, A.; Joosten, H. J.; Finnigan, J.; Charnock, S.; Fessner, W. D. nanoDSF as screening tool for enzyme libraries and biotechnology development. *FEBS J.* **2019**, *286* (1), 184–204.
- (49) Linke, P.; Amaning, K.; Maschberger, M.; Vallee, F.; Steier, V.; Baaske, P.; Duhr, S.; Breitsprecher, D.; Rak, A. An Automated Microscale Thermophoresis Screening Approach for Fragment-Based Lead Discovery. *J. Biomol. Screen* **2016**, *21* (4), 414–421.
- (50) Zorn, K. M.; Lane, T. R.; Russo, D. P.; Clark, A. M.; Makarov, V.; Ekins, S. Multiple Machine Learning Comparisons of HIV Cell-based and Reverse Transcriptase Data Sets. *Mol. Pharm.* **2019**, *16* (4), 1620–1632.
- (51) Russo, D. P.; Zorn, K. M.; Clark, A. M.; Zhu, H.; Ekins, S. Comparing Multiple Machine Learning Algorithms and Metrics for Estrogen Receptor Binding Prediction. *Mol. Pharm.* **2018**, *15* (10), 4361–4370.
- (52) Dolisca, S. B.; Mehta, M.; Pearce, D. A.; Mink, J. W.; Maria, B. L. Batten disease: clinical aspects, molecular mechanisms, translational science, and future directions. *J. Child Neurol.* **2013**, *28* (9), 1074–1100.
- (53) Yap, S. Q.; Mathavarajah, S.; Huber, R. J. The converging roles of Batten disease proteins in neurodegeneration and cancer. *iScience* **2021**, *24* (4), 102337.

- (54) Zhou, B.; Hao, Q.; Liang, Y.; Kong, E. Protein palmitoylation in cancer: molecular functions and therapeutic potential. *Mol. Oncol.* **2023**, *17* (1), 3–26.
- (55) Padwal, R. S.; Majumdar, S. R. Drug treatments for obesity: orlistat, sibutramine, and rimonabant. *Lancet* **2007**, *369* (9555), 71–77.
- (56) Hill, T. K.; Davis, A. L.; Wheeler, F. B.; Kelkar, S. S.; Freund, E. C.; Lowther, W. T.; Kridel, S. J.; Mohs, A. M. Development of a Self-Assembled Nanoparticle Formulation of Orlistat, Nano-ORL, with Increased Cytotoxicity against Human Tumor Cell Lines. *Mol. Pharm.* **2016**, *13* (3), 720–728.
- (57) You, B. J.; Chen, L. Y.; Hsu, P. H.; Sung, P. H.; Hung, Y. C.; Lee, H. Z. Orlistat Displays Antitumor Activity and Enhances the Efficacy of Paclitaxel in Human Hepatoma Hep3B Cells. *Chem. Res. Toxicol.* **2019**, *32* (2), 255–264.
- (58) Czumaj, A.; Zabielska, J.; Pakiet, A.; Mika, A.; Rostkowska, O.; Makarewicz, W.; Kobiela, J.; Sledzinski, T.; Stelmanska, E. *In Vivo* Effectiveness of Orlistat in the Suppression of Human Colorectal Cancer Cell Proliferation. *Anticancer Res.* **2019**, *39* (7), 3815–3822.
- (59) Chuang, H. Y.; Lee, Y. P.; Lin, W. C.; Lin, Y. H.; Hwang, J. J. Fatty Acid Inhibition Sensitizes Androgen-Dependent and -Independent Prostate Cancer to Radiotherapy via FASN/NF- $\kappa$ B Pathway. *Sci. Rep.* **2019**, *9* (1), 13284.
- (60) Cioccoloni, G.; Aquino, A.; Notarnicola, M.; Caruso, M. G.; Bonmassar, E.; Zonfrillo, M.; Caporali, S.; Faraoni, I.; Villiva, C.; Fuggetta, M. P.; Franzese, O. Fatty acid synthase inhibitor orlistat impairs cell growth and down-regulates PD-L1 expression of a human T-cell leukemia line. *J. Chemother.* **2020**, *32* (1), 30–40.
- (61) Lv, K.; Ren, J. G.; Han, X.; Gui, J.; Gong, C.; Tong, W. Depalmitoylation rewires FLT3-ITD signaling and exacerbates leukemia progression. *Blood* **2021**, *138* (22), 2244–2255.
- (62) Camara, K.; Kamat, S. S.; Lasota, C. C.; Cravatt, B. F.; Howell, A. R. Combining cross-metathesis and activity-based protein profiling: New  $\beta$ -lactone motifs for targeting serine hydrolases. *Bioorg. Med. Chem. Lett.* **2015**, *25* (2), 317–321.
- (63) Xu, J.; Su, Z.; Cheng, X.; Hu, S.; Wang, W.; Zou, T.; Zhou, X.; Song, Z.; Xia, Y.; Gao, Y.; Zheng, Q. High PPT1 expression predicts poor clinical outcome and PPT1 inhibitor DC661 enhances sorafenib sensitivity in hepatocellular carcinoma. *Cancer Cell Int.* **2022**, *22* (1), 115.
- (64) Lane, T. R.; Dyllal, J.; Mercer, L.; Goodin, C.; Foil, D. H.; Zhou, H.; Postnikova, E.; Liang, J. Y.; Holbrook, M. R.; Madrid, P. B.; Ekins, S. Repurposing Pyramax<sup>®</sup>, quinacrine and tilorone as treatments for Ebola virus disease. *Antiviral Res.* **2020**, *182*, 104908.
- (65) Pisonero-Vaquero, S.; Medina, D. L. Lysosomotropic Drugs: Pharmacological Tools to Study Lysosomal Function. *Curr. Drug Metab.* **2018**, *18* (12), 1147–1158.
- (66) Nentwig, T. B.; Obray, J. D.; Vaughan, D. T.; Chandler, L. J. Behavioral and slice electrophysiological assessment of DREADD ligand, deschloroclozapine (DCZ) in rats. *Sci. Rep.* **2022**, *12* (1), 6595.
- (67) Snell, J.; Swersky, K.; Zemel, R. S. Prototypical Networks for Few-shot Learning. *arXiv (Computer Science.Machine Learning)*, June 19, 2017, 1703.05175, ver. 2. <https://arxiv.org/abs/1703.05175>.
- (68) Lu, J. Y.; Hu, J.; Hofmann, S. L. Human recombinant palmitoyl-protein thioesterase-1 (PPT1) for preclinical evaluation of enzyme replacement therapy for infantile neuronal ceroid lipofuscinosis. *Mol. Genet. Metab.* **2010**, *99* (4), 374–378.
- (69) Puhl, A. C.; Mottin, M.; Sacramento, C. Q.; Tavella, T. A.; Dias, G. G.; Fintelman-Rodrigues, N.; Temerozo, J. R.; Dias, S. S. G.; Ramos, P. R. P. D.; Merten, E. M.; Pearce, K. H.; Costa, F. T. M.; Premkumar, L.; Souza, T. M. L.; Andrade, C. H.; Ekins, S. Computational and Experimental Approaches Identify Beta-Blockers as Potential SARS-CoV-2 Spike Inhibitors. *ACS Omega* **2022**, *7* (32), 27950–27958.
- (70) Puhl, A. C.; Fritch, E. J.; Lane, T. R.; Tse, L. V.; Yount, B. L.; Sacramento, C. Q.; Fintelman-Rodrigues, N.; Tavella, T. A.; Maranhão Costa, F. T.; Weston, S.; Logue, J.; Frieman, M.; Premkumar, L.; Pearce, K. H.; Hurst, B. L.; Andrade, C. H.; Levi, J. A.; Johnson, N. J.; Kisthardt, S. C.; Scholle, F.; Souza, T. M. L.; Moorman, N. J.; Baric, R. S.; Madrid, P. B.; Ekins, S. Repurposing the Ebola and Marburg Virus Inhibitors Tilorone, Quinacrine, and Pyronaridine: *In Vitro* Activity against SARS-CoV-2 and Potential Mechanisms. *ACS Omega* **2021**, *6* (11), 7454–7468.
- (71) Clark, A. M.; Dole, K.; Coulon-Spektor, A.; McNutt, A.; Grass, G.; Freundlich, J. S.; Reynolds, R. C.; Ekins, S. Open Source Bayesian Models. 1. Application to ADME/Tox and Drug Discovery Datasets. *J. Chem. Inf. Model.* **2015**, *55* (6), 1231–1245.
- (72) Clark, A. M.; Ekins, S. Open Source Bayesian Models. 2. Mining a “Big Dataset” To Create and Validate Models with ChEMBL. *J. Chem. Inf. Model.* **2015**, *55* (6), 1246–1260.
- (73) Lane, T.; Russo, D. P.; Zorn, K. M.; Clark, A. M.; Korotcov, A.; Tkachenko, V.; Reynolds, R. C.; Perryman, A. L.; Freundlich, J. S.; Ekins, S. Comparing and Validating Machine Learning Models for Mycobacterium tuberculosis Drug Discovery. *Mol. Pharm.* **2018**, *15* (10), 4346–4360.
- (74) Sandoval, P. J.; Zorn, K. M.; Clark, A. M.; Ekins, S.; Wright, S. H. Assessment of Substrate-Dependent Ligand Interactions at the Organic Cation Transporter OCT2 Using Six Model Substrates. *Mol. Pharmacol.* **2018**, *94* (3), 1057–1068.
- (75) Clark, A. M.; Dole, K.; Coulon-Spektor, A.; McNutt, A.; Grass, G.; Freundlich, J. S.; Reynolds, R. C.; Ekins, S. Open source bayesian models: 1. Application to ADME/Tox and drug discovery datasets. *J. Chem. Inf. Model.* **2015**, *55*, 1231–1245.
- (76) Clark, A. M.; Ekins, S. Open Source Bayesian Models: 2. Mining A “big dataset” to create and validate models with ChEMBL. *J. Chem. Inf. Model.* **2015**, *55*, 1246–1260.
- (77) Carletta, J. Assessing agreement on classification tasks: The kappa statistic. *Comput. Ling.* **1996**, *22*, 249–254.
- (78) Cohen, J. A coefficient of agreement for nominal scales. *Educ. Psychol. Meas.* **1960**, *20*, 37–46.
- (79) Matthews, B. W. Comparison of the predicted and observed secondary structure of T4 phage lysozyme. *Biochim. Biophys. Acta* **1975**, *405* (2), 442–451.